

Broadband Optical Phase Modulation by Colloidal CdSe Quantum Wells

Ivo Tanghe, Justinas Butkus, Kai Chen, Ronnie R. Tamming, Shalini Singh, Yera Ussembayev, Kristiaan Neyts, Dries van Thourhout, Justin M. Hodgkiss, and Pieter Geiregat*



Cite This: *Nano Lett.* 2022, 22, 58–64



Read Online

ACCESS |



Metrics & More



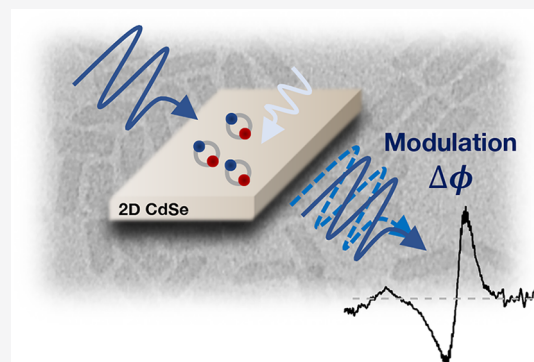
Article Recommendations



Supporting Information

ABSTRACT: Two-dimensional (2D) semiconductors are primed to realize a variety of photonic devices that rely on the transient properties of photogenerated charges, yet little is known on the change of the refractive index. The associated optical phase changes can be beneficial or undesired depending on the application, but require proper quantification. Measuring optical phase modulation of dilute 2D materials is, however, not trivial with common methods. Here, we demonstrate that 2D colloidal CdSe quantum wells, a useful model system, can modulate the phase of light across a broad spectrum using a femtosecond interferometry method. Next, we develop a toolbox to calculate the time-dependent refractive index of colloidal 2D materials from widely available transient absorption experiments using a modified effective medium algorithm. Our results show that the excitonic features of 2D materials result in broadband, ultrafast, and sizable phase modulation, even extending to the near infrared because of intraband transitions.

KEYWORDS: 2D materials, spectroscopy, optical phase, nanocrystals



In the past decade, inorganic nanoscale materials have been shown to be attractive materials to fabricate solution-processable optoelectronic devices.^{1,2} Several groups have used their remarkable light–matter coupling to realize both cost and energy-efficient operation, e.g. as light-emitting diodes and integrated lasers.^{1,3–5} In particular, materials that show strong room-temperature excitonic features, such as two-dimensional (2D) nanoplatelets (NPLs)^{6,7} or transition-metal dichalcogenides (TMDs),⁸ are highly desired as they combine inter- and intraband transitions with narrow line widths and large oscillator strengths.⁹ To date, a very thorough understanding has been built up regarding the interaction of light with these materials.^{7,8,10} In particular, the effect of photoexcitations on the way light is absorbed or emitted has been studied, which is key to designing light-absorbing, -emitting, and -amplifying composite media.^{11,12}

However, light is more than the intensity of the electric field. Many photonic devices rely on materials to achieve manipulation of the phase. Examples include mode-locked lasers, ultrafast on-chip modulators, etc.^{13,14} Strong modulations of the (real part of the) refractive index Δn of an embedded material impart a phase change $\Delta\phi$ ($\propto\Delta n$) when light propagates through the device. Such modulations are obtained when, for example, charge carriers are generated, either electrically or optically, which leads to strong changes of the absorbance and, by virtue of the Kramers–Kronig relations, to changes in the real part of the refractive index.¹⁵

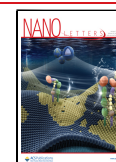
Phase shifts are sometimes also unwanted, such as for high Q-factor photonic cavities^{3,11} or waveguiding thin film devices such as solar concentrators.¹⁶ In this context, a small index change can drastically alter the local photonic density of states, impacting light confinement or propagation.^{16–18} Similarly, the analysis of transient absorption experiments on thin films are often complicated by transient photorefractive effects.^{19,20}

Clearly, a proper quantification of refractive index changes present in 2D materials is desired. As mentioned above, modulation of the refractive index entices a phase change. Such changes are difficult to measure as most detection schemes rely on intensity. Moreover, most of the high-quality colloidal dispersed 2D materials, such as II–VI NPLs,^{6,10} perovskite quantum wells^{21,22} or colloidal TMDs,^{23,24} are obtained in dilute ensembles, such as colloidal dispersions, which implies only small modifications of the composite’s total refractive index will be observed. The question thus arises of how the strong excitonic nature of optical transitions found in (colloidal) two-dimensional materials can transiently affect

Received: August 17, 2021

Revised: December 4, 2021

Published: December 29, 2021



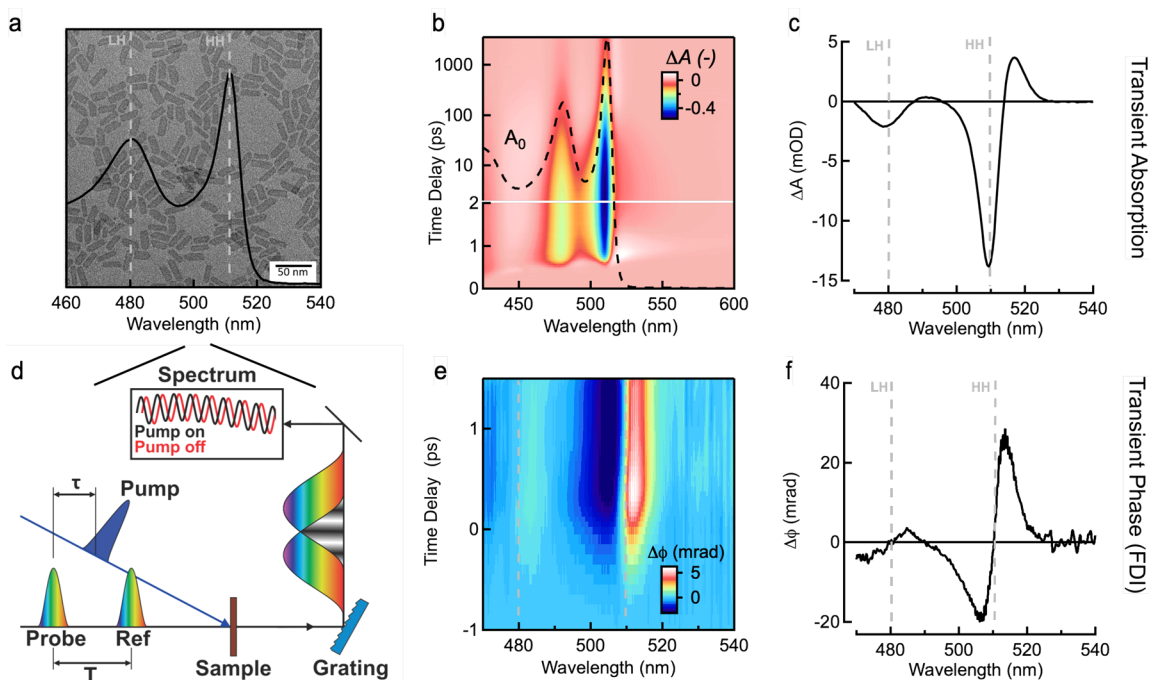


Figure 1. Experimental observation of phase modulation by CdSe nanoplatelets (NPLs) (a) Transmission electron microscopy (TEM) image of the NPLs used in this work. Inset shows the linear absorption spectrum with heavy (HH) and light (LH) hole exciton transitions indicated. (top) (b) 2D false color map of the change in absorbance ΔA measured after photoexcitation with 400 nm. (c) Spectral slice at 1 ps time delay showing distinct bleach features at the HH and LH positions. (d) Schematic of the frequency domain interference (FDI) setup used in this work where two probe replicas are projected onto an array detector. From the interference pattern, the phase change induced by optically pumping the NPL dispersion can be extracted. (e) 2D false color map of the differential phase $\Delta\phi$ as a function of probe wavelength and time for 4.5 ML CdSe NPLs after excitation with 400 nm. (f) Spectral slice of the phase change $\Delta\phi$ (mrad) at a time delay of 1 ps. We note that the zero-crossing points correspond to the HH/LH positions, as indicated by the gray dashed lines.

the phase of light and how this change can be measured in a reliable fashion.

Herein, we present a study of the ultrafast phase modulation of colloidal 2D CdSe quantum wells or nanoplatelets (NPLs), as a reference 2D system with interband exciton features in the visible part of the spectrum and intraband features in the near infrared.^{6,7} First, we use a femtosecond frequency domain interferometry (FDI) method to show experimentally that broadband and sizable optical phase modulation takes place after photoexcitation. Given the limitations of the FDI method, we proceed to develop a framework to extract phase modulation information over arbitrary time and wavelength spans. Next, we show that the linear refractive index of 2D materials can be extracted directly from the linear absorption spectrum of a colloidal solution. Using this information, we develop a routine to translate broadband transient absorption (TA) experiments into equally broadband “transient phase” experiments. A cross-check with the FDI method confirms that our algorithm is consistent. Proceeding with this methodology, we reveal particularly strong on- and off-resonance modulations of the refractive index. Finally, our experiments also suggest the possibility of technologically relevant near-infrared phase modulation using spectrally narrow intraband transitions.

CdSe NPLs are obtained through a colloidal synthesis as scatter-free dispersions with high luminescence quantum yields up to 80%, see also Supporting Information S2.^{6,25,26} Figure 1a shows a transmission electron microscopy (TEM) image of the sample used, showing a lateral area of $34 \times 9.6 \text{ nm}^2$. The thickness is atomically defined at 4.5 monolayers of CdSe (1.37 nm).^{8,9} The overlay of Figure 1a shows the linear absorption

spectrum of the platelets dispersed in hexane. The spectrum is composed of typical II–VI semiconductor exciton transitions related to heavy (HH, 510 nm) and light hole (LH, 480 nm) states coupled to the same conduction band level.^{6,10,27} We note that no subgap scattering occurs, effectively putting the extinction to zero for all wavelengths beyond ca. 520 nm.

First, we use femtosecond transient absorption (TA) spectroscopy to study the effect of photogenerated charges on the optical transitions. In these commonly used experiments, a short 110 fs pulse at 400 nm is used to photoexcite the CdSe NPLs in solution creating, after rapid thermalization, a number $\langle N \rangle$ of heavy-hole excitons, see Supporting Information S3.1. Next, a broadband probe pulse, orthogonal in polarization to the pump (see Supporting Information S3.3), measures the change of absorbance $\Delta A(\lambda, t)$ which is resolved in time and wavelength, as is shown in Figure 1b using a false color map. Figure 1c shows a spectral slice of the TA map at 1 ps, where we observe strong bleach features ($\Delta A < 0$) at the heavy and light-hole exciton lines due to state filling and an induced absorption due to exciton-biexciton transitions.²⁸ The absorption (change) is connected to the imaginary part k of the complex refractive index $\tilde{n} = n + ik$. Consequently, a sizable modulation of the real part of the refractive index n could be expected, as both are connected through the Kramers–Kronig relationship.

To verify our expectation, we experimentally demonstrate refractive index modulation Δn by measuring the ensuing optical phase modulation $\Delta\phi$ ($\propto \Delta n$) imparted on a colloidal dispersion of NPLs. Following the method initially conceived by Tokunaga²⁹ and optimized by Tamming et al.,¹⁸ we measure the phase change of a broadband probe beam using

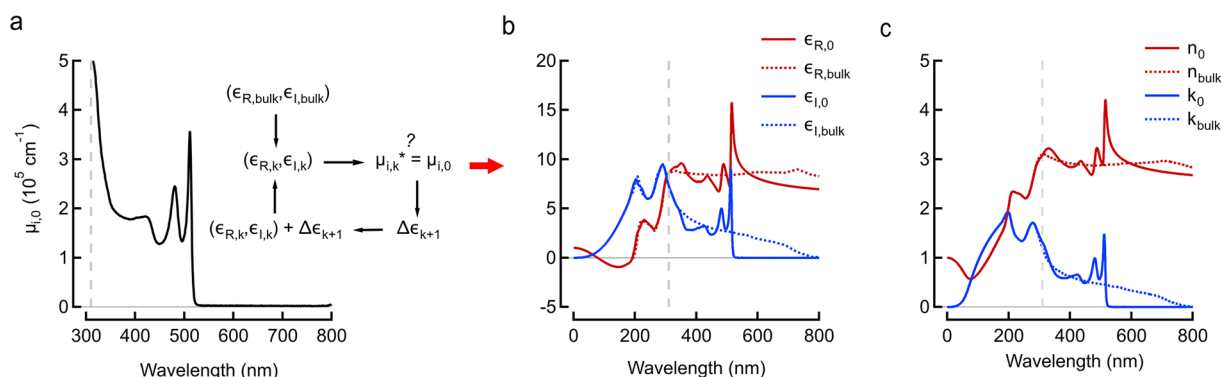


Figure 2. Steady-state complex refractive index of CdSe NPLs. (a) Ground state absorption spectrum plotted as the intrinsic absorption coefficient $\mu_{i,0}$. Inset shows a summary of the iterative procedure used to translate the $\mu_{i,0}$ spectrum into the permittivity function $\tilde{\epsilon}_0$, which is shown in panel b. Dotted lines indicate the bulk dielectric function of CdSe. (c) Calculated complex linear refractive index $\tilde{n}_0 = n_0 + ik_0$ of the NPLs from the permittivity function in panel b. The (complex) bulk CdSe refractive index is shown in dotted lines as reference. The vertical gray dashed line indicates the 4 eV point from which the dielectric function is assumed to be bulk-like toward shorter wavelengths.

frequency domain interference (FDI). In short, a probe beam is split in a pair of reference and detection beams using a Michelson interferometer and follow the same optical path through the sample and spectrometer to produce interference fringes on a multichannel detector, see Figure 1d. The reference pulse arrives at the sample approximately 2 ps before the probe, with the pump arriving between the probe and reference, such that only the probe interacts with the excited sample. Thus, photoinduced changes to the sample refractive index results in a phase shift of the interference fringes, which is recovered as a phase-shift spectrum.

Figure 1e shows a false color map of the differential phase $\Delta\phi$ obtained after 400 nm photoexcitation with $\langle N \rangle = 4.7$. We note that the phase change entices that of the composite medium, being NPLs in hexane. Because hexane is not responsive to the 400 nm pump, we assign this phase change to a change of the dispersed NPL's refractive index. However, the composite dielectric nature of the composite medium (m) does not allow us to directly link this measured composite medium phase change to the refractive index change of the NPLs themselves, a point we will come back to further. Indeed, the phase change in a composite medium with path length L is the consequence of the medium's refractive index change (Δn_m) and can be written as

$$\Delta\phi = \Delta n_m(\Delta n, n_s, f) \frac{2\pi}{\lambda} L \quad (1)$$

where Δn is the modulation of the real part of the NPL's complex refractive index \tilde{n} , n_s is the solvent refractive index, and f is the volume fraction of NPLs in the dispersion. Figure 1f shows the phase shift spectrum at 1 ps, indicating that strong modulations take place around the heavy and light-hole resonances. Clear zero-crossings correspond to the bleach and absorption maxima at the HH and LH positions.

Clearly, sizable and broadband phase modulation is possible using CdSe NPLs. However, FDI requires a high spectral resolution. Therefore, the grating dispersion, sensor's pixel size, and achievable probe spectral density are severe limitations resulting in a detection up to 1.5 ps time-delay only and a narrow 40 nm spectral window. Broader spectra can be obtained by stitching probe windows. To overcome these limitations, we proceed to develop an algorithm to use the more extensive TA data sets directly.

To extract the real part of the refractive index, we can rely on the Kramers–Krönig (KK) relations, which connect real and imaginary parts of a material's refractive index. Despite the simple premise of the KK relations, the experimentally accessible absorption spectrum of colloids is not trivially connected to the dielectric function $\tilde{\epsilon}$, or equivalently the complex refractive index $\tilde{n} = \tilde{\epsilon}_{1/2}$, of the material. NPLs in particular consist of an inorganic core and a shell of organic ligands, dispersed in a transparent, low-permittivity solvent. Such a composite nature complexes the analytical expressions connecting absorption to the refractive index and vice versa. One can write down an analytical expression for the accessible intrinsic absorption coefficient $\mu_i = \frac{\ln(10)A_0}{fL}$, see Figure 2a and Supporting Information S4–S4.2, for randomly oriented NPL absorbers, which is connected to the dielectric parameters of the nanoparticle ($\tilde{\epsilon} = \epsilon_R + i\epsilon_I$) and the solvent (ϵ_s) through the Maxwell–Garnett effective medium approach:³⁰

$$\mu_i = \frac{2\pi}{\sqrt{\epsilon_s}\lambda} \frac{1}{3} (|f_{LF,x}|^2 + |f_{LF,y}|^2 + |f_{LF,z}|^2) \epsilon_I \quad (2)$$

where ϵ_I is the imaginary part of the NPL refractive index, λ is the wavelength of interest, and $f_{LF,i}$ is the local field factor along the different spatial directions. Using an electrostatic approximation, we can write the local field factors explicitly depending on the shape of the nanoparticle:

$$f_{LF,i} = \frac{\epsilon_s}{\epsilon_s + L_i(\tilde{\epsilon} - \epsilon_s)} \quad (3)$$

where L_i is called a depolarization factor and ϵ_s is the solvent dielectric function. Clearly, the complex dependence of f_{LF} does not allow a straightforward extraction of $\tilde{\epsilon}_0$ from $\mu_{i,0}$. However, several groups showed that it is still possible to extract the complex dielectric function for zero-dimensional quantum dots (QDs) when making only a few assumptions.^{31,32} First, the dielectric function is taken as equal to the bulk dielectric function at high energy, here for example below 310 nm, an assumption that formed the basis of the calculation of $\mu_{i,0}$ from theory and was shown experimentally to be valid.^{30,33,34} Next, we know that the dielectric function has a zero imaginary part at photon energies below the band gap, as observed experimentally because of zero absorbance. Combining the above considerations, one can devise an iterative procedure to extract the NPL dielectric function based on a

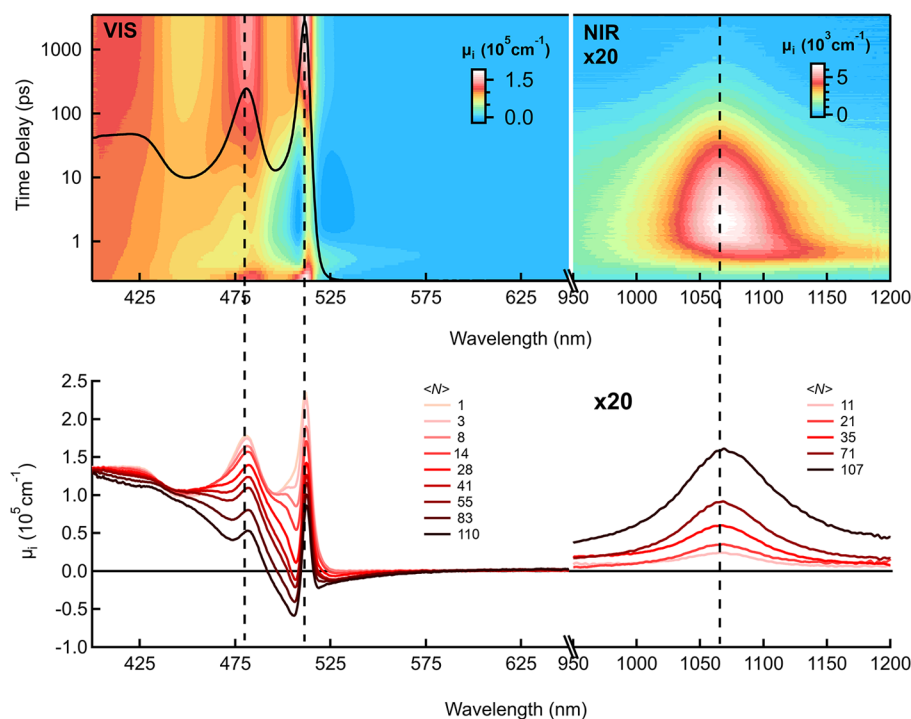


Figure 3. Overview of $\mu_i(\lambda, t)$ nonlinear absorption spectroscopy. (Top) False color map of μ_i across the visible and near-infrared spectrum. (Bottom) Slices of the color maps at 3 ps for increasing fluence, expressed as an average number of absorbed photons per NPL, $\langle N \rangle$. Note that for the top and bottom, the infrared response has been scaled by a factor 20.

cycle of perturbations of the bulk dielectric function, subscript b, using the KK relations and comparisons of the resulting calculated μ_i with the experimental one in each iteration step (k), see inset Figure 2a. As laid out by several groups,^{31,32} these perturbations were obtained from a linearized version of the Maxwell-Garnett (MG) relations. This approach has resulted in excellent convergence and detailed knowledge of the dielectric function of quantum dots.^{31,32}

We adapted this procedure to include generalized depolarization factors that depend strongly on the shape of the NPLs. Supporting Information S4 discusses in detail the flow and complications of this modified procedure. Figure 2b,c shows the result by plotting the complex linear (subscript 0) permittivity $\tilde{\epsilon}_0 = \epsilon_{R,0} + i\epsilon_{I,0}$ and refractive index $\tilde{n}_0 = n_0 + ik_0$. We can see small deviations from the bulk refractive index and permittivity at short wavelengths (dashed lines) and strong derivative-like features around the heavy- and light-hole exciton features. Our results are in good agreement with a recent report from Zhang et al., who used ellipsometry on thin films of nanoplatelets.³⁵ We note that the refractive index calculated using the algorithm method is the index of the nanoplatelets themselves, independent of the environment.

On the basis of the excellent convergence of the KK algorithm, we now have a procedure to go from normalized absorption spectra to the complex refractive index \tilde{n} and eventually the desired real part n . Such spectra are exactly offered by transient absorption spectroscopy on ultrafast time scales. Indeed, we can normalize the transient absorbance $A(\lambda, t) (= A_0(\lambda) + \Delta A(\lambda, t))$ spectra to represent $\mu_i(\lambda, t)$, the time-dependent and nonlinear intrinsic absorption coefficient.^{10,36,37}

Figure 3 (top) shows a typical color map of $\mu_i(\lambda, t)$ across the visible and near-infrared spectrum for $\langle N \rangle \approx 110$. Every horizontal slice of this map represents a normalized absorption spectrum that can be converted into a \tilde{n} spectrum using the

algorithm outlined above. As such, a complex \tilde{n} will be a time- and wavelength-dependent quantity $\tilde{n}(\lambda, t) = n(\lambda, t) + ik(\lambda, t)$. In a final step, we can calculate back the change of real part of the refractive index Δn , as $\Delta n(\lambda, t) = n(\lambda, t) - n_0(\lambda)$. The latter is required to calculate the phase change of the composite medium, see eq 1, and cross-check our algorithm with the FDI measurements of Figure 1.

Focusing first on the $\mu_i(\lambda, t)$ input, we show in Figure 3 (bottom) a summary of the fluence dependence at 3 ps in the visible and near-infrared part of the spectrum. Similar to the observations of Tomar et al., we observe an increased saturation of the HH/LH absorption.¹⁰ The absorbance also turns negative, indicating the occurrence of net optical gain.^{5,10,12} In the near-infrared, we observe the clear emergence of the well-defined intraband transition (IB). As confirmed by Diroll et al., we can assign this feature to an electron-related intraband transition.³⁸

Figure 4a shows the calculated map of $\Delta n = n - n_0$, i.e., the change in the real part of the refractive index of the NPLs, together with n_0 , the linear refractive index (black line), for $\langle N \rangle = 110$, equivalent to a surface carrier density of $4.5 \times 10^{13} \text{ cm}^{-2}$. We should note that this density corresponds most likely to a mixture of free charges, excitons, and biexcitons.¹⁰ We observe a clear connection to the bleach features of Figure 1b as derivative signatures are observed around the HH and LH exciton positions (485 nm/512 nm). Extending into the near infrared, a sizable modulation is also observed around IB. Moreover, a broad sub-band gap modulation is observed in the region of 550–950 nm, where no steady-state absorption is present.

We note that our model yields the modulation of the NPL refractive index and is as such an intrinsic change at the level of the nanoparticle. To directly compare this to the phase shift of the FDI experiments, we need to calculate the effect of a

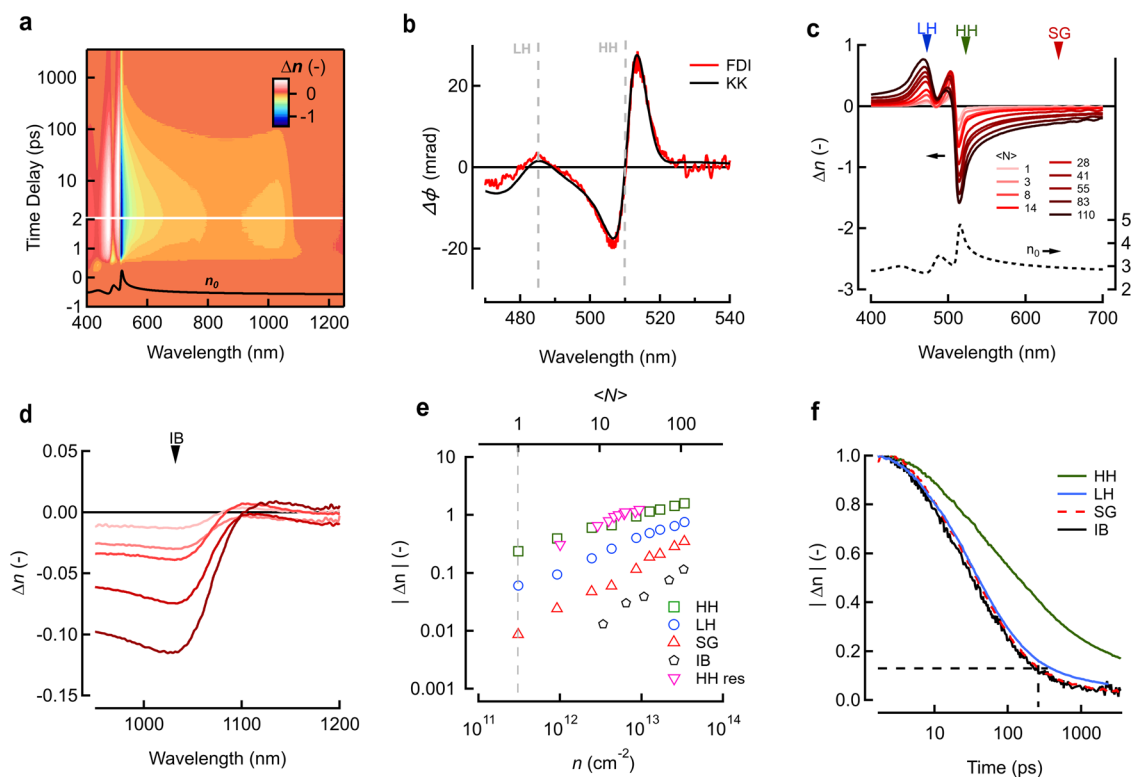


Figure 4. (a) False color map of the transient refractive index of 4.5 ML CdSe NPLs obtained via the KK methodology. (b) Comparison of the phase change between the FDI experiment (red) and the KK model from TA data (black), evaluated at 1 ps. (c) Fluence-dependent refractive index modulation of CdSe NPLs evaluated at 3 ps for increasing exciton density expressed by $\langle N \rangle$ for the (c) visible and (d) near-infrared spectrum. (e) Carrier density scaling of the refractive index modulation Δn at 3 ps for select wavelengths (see arrows in c and d) for excitation at 400 nm: the light-hole resonance (470 nm), the heavy-hole resonance (513 nm), the subgap region (600 nm), and the intraband transition (1050 nm). The vertical dashed line indicates the regime of 1 excitation per NPL. Pink triangles indicate the response for 510 nm resonant excitation probed at the heavy-hole position. (f) Normalized kinetics of the Δn at the select wavelengths. The horizontal dashed line indicates the $1/e^2$ point used to extract the limit for the modulation time constant (318 ps).

change in the NPL refractive index Δn on the whole composite medium (solvent, NPLs) measured using FDI. Figure 4b shows the comparison between the experimental FDI phase change (red) and the phase change obtained from our algorithm approach, see Supporting Information S6. Both the magnitude, the sharp derivative shape figures around the HH/LH resonances, and the subgap modulation of the phase shift are retrieved quantitatively. This excellent match again confirms that we can use the iterative algorithm presented earlier to obtain the absolute (and transient) refractive index (changes) reliably.

Having confirmed the KK approach, we proceed in Figure 4c, d to show the spectra of Δn at 3 ps for increasing carrier densities. Figure 4e shows the fluence scaling at select wavelengths indicated in Figures 4c, d: at the HH resonance (510 nm, $n_0 = 3.45$), the LH resonance (485 nm, $n_0 = 3.2$), the sub-band gap (600 nm, $n_0 = 2.9$), and the near-infrared intraband transition (IB, 1050 nm, $n_0 = 2.7$). First off, we observe above-unity modulation at high carrier density for HH, corresponding to $\Delta n/n_0 > 0.3$. Tomar et al. showed that optical gain occurs in that spectral range so clearly these modulations will affect cavity design for lasers based on these materials.¹¹ On the LH resonance, the modulation is equally intense leveling off at around $\Delta n \approx 1$. For the subgap modulation at, e.g., 600 nm, a maximum relative change $\Delta n/n_0 = 0.13$ is observed. Finally, we also report on resonant pump (510 nm) experiments in the Supporting Information S3.2 that indicate even stronger modulations are possible. Increased

saturation of the exciton lines for cold charges lie at the root of these observations. We highlight that the modulations keep scaling with carrier density, even if the composition of the latter changes from purely excitonic to an admixture with free charges and biexciton complexes.

It is worthwhile to compare the values of index modulation obtained to literature reports on 2D systems, such as epitaxial quantum wells or TMDs.^{39–41} Typical refractive index changes are limited to 0.01 for off-resonance and to 0.1 for on-resonance modulation for carrier densities generated electrically close to $1 \times 10^{13} \text{ cm}^{-2}$. For our experimental scenario NPLs offer stronger modulations at comparable surface density and even exceed epitaxial 2D materials for resonant modulations. The work of Park et al. showed that decreasing quantum well thickness down to ca. 7 nm improves the modulation depth at fixed carrier density, an effect ascribed to the increased excitonic character of the band edge transitions. The even stronger modulation observed here for the extremely thin 1.37 nm CdSe quantum wells fits within that concept, indicating the importance of excitonic effects.

Rapid multiexciton recombination will quench the modulation,⁴² yet Figure 4e shows that even for regimes of single excitations per sheet (vertical dashed line) $\langle N \rangle \ll 1$, or sheet densities below $1 \times 10^{11} \text{ cm}^{-2}$, a sizable modulation is achievable. Figure 4f shows the full kinetics at the same select wavelengths as Figure 4e for a fluence creating $\langle N \rangle = 110$.^{5,42–44} On the basis of the $1/e^2$ limit, shown as the horizontal dashed line in Figure 4f, modulations should be

feasible at a rate close 3.5 GHz (285 ps) across a wide spectral window.

In summary, a framework to measure and calculate the steady-state and transient complex refractive index of colloidal 2D semiconductors, from routine UV/vis and TA data, respectively, was presented and cross-checked experimentally using frequency domain interferometry. As a case example, we identified ultrafast, broadband, and strong phase modulation in colloidal 2D CdSe quantum wells. We argue that the highly excitonic nature of the optical transitions is responsible for the broad and sizable nature of these effects. The narrow intraband features of atomically precise 2D materials furthermore open up exciting possibilities of substantial and fast phase modulation in the near-infrared range.

■ ASSOCIATED CONTENT

SI Supporting Information

The Supporting Information is available free of charge at <https://pubs.acs.org/doi/10.1021/acs.nanolett.1c03181>.

Material synthesis and characterization, the iterative algorithm, and the ultrafast spectroscopy experiments (PDF)

■ AUTHOR INFORMATION

Corresponding Author

Pieter Geiregat – *Physics and Chemistry of Nanostructures, Department of Chemistry and Center for Nano and Biophotonics, Ghent University, Gent 9000, Belgium;* orcid.org/0000-0001-7217-8738;
Email: Pieter.Geiregat@UGent.be

Authors

Ivo Tanghe – *Photonics Research Group, Ghent University, Gent 9000, Belgium; Physics and Chemistry of Nanostructures, Department of Chemistry and Center for Nano and Biophotonics, Ghent University, Gent 9000, Belgium*

Justinas Butkus – *School of Chemical and Physical Sciences, Victoria University of Wellington, Wellington 6012, New Zealand; The Dodd-Walls Centre for Photonic and Quantum Technologies, Dunedin 9016, New Zealand; MacDiarmid Institute for Advanced Materials and Nanotechnology, Wellington 6012, New Zealand*

Kai Chen – *Robinson Research Institute, Faculty of Engineering, Victoria University of Wellington, Wellington 6012, New Zealand; The Dodd-Walls Centre for Photonic and Quantum Technologies, Dunedin 9016, New Zealand; MacDiarmid Institute for Advanced Materials and Nanotechnology, Wellington 6012, New Zealand*

Ronnie R. Tammimg – *School of Chemical and Physical Sciences, Victoria University of Wellington, Wellington 6012, New Zealand; Robinson Research Institute, Faculty of Engineering, Victoria University of Wellington, Wellington 6012, New Zealand; MacDiarmid Institute for Advanced Materials and Nanotechnology, Wellington 6012, New Zealand*

Shalini Singh – *Department of Chemical Sciences and Bernal Institute, University of Limerick, Limerick V94 T9PX, Ireland;* orcid.org/0000-0001-8607-8383

Yera Ussembayev – *Liquid Crystals and Photonics Research Group, Department of Electronics and Information Systems,*

Ghent University, Gent 9000, Belgium; orcid.org/0000-0002-4779-9046

Kristiaan Neyts – *Liquid Crystals and Photonics Research Group, Department of Electronics and Information Systems, Ghent University, Gent 9000, Belgium;* orcid.org/0000-0001-5551-9772

Dries van Thourhout – *Photonics Research Group, Ghent University, Gent 9000, Belgium; Center for Nano and Biophotonics, Ghent University, Gent 9000, Belgium;* orcid.org/0000-0003-0111-431X

Justin M. Hodgkiss – *School of Chemical and Physical Sciences, Victoria University of Wellington, Wellington 6012, New Zealand; MacDiarmid Institute for Advanced Materials and Nanotechnology, Wellington 6012, New Zealand;* orcid.org/0000-0002-9629-8213

Complete contact information is available at:

<https://pubs.acs.org/10.1021/acs.nanolett.1c03181>

Notes

The authors declare no competing financial interest.

■ ACKNOWLEDGMENTS

The authors acknowledge the FWO-Vlaanderen (G.0760.12, 12K8216N). J.M.H. and K.C. acknowledge support from the Marsden Fund.

■ REFERENCES

- (1) Kovalenko, M. V.; Manna, L.; Cabot, A.; Hens, Z.; Talapin, D. V.; Kagan, C. R.; Klimov, V. I.; Rogach, A. L.; Reiss, P.; Milliron, D. J.; Guyot-sionnest, P.; Konstantatos, G.; Parak, W. J.; Hyeon, T.; Korgel, B. A.; Murray, C. B.; Heiss, W. Prospects of Nanoscience with Nanocrystals. *ACS Nano* **2015**, *9*, 1012–1057.
- (2) Kagan, C. R.; Lifshitz, E.; Sargent, E. H.; Talapin, D. V. Building devices from colloidal quantum dots. *Science* **2016**, *353*, 885.
- (3) Xie, W.; Stoflerle, T.; Raino, G.; Aubert, T.; Bisschop, S.; Zhu, Y.; Mahrt, R. F.; Geiregat, P.; Brainin, E.; Hens, Z.; Van Thourhout, D. On-Chip Integrated Quantum-Dot–Silicon-Nitride Microdisk Lasers. *Adv. Mater.* **2017**, *29*, 1604866.
- (4) Xie, W.; Zhu, Y.; Bisschop, S.; Aubert, T.; Hens, Z.; van Thourhout, D.; Geiregat, P. Colloidal Quantum Dots Enabling Coherent Light Sources for Integrated Silicon-Nitride Photonics. *IEEE J. Sel. Top. Quantum Electron.* **2017**, *23*, 1–13.
- (5) Geiregat, P.; Van Thourhout, D.; Hens, Z. A bright future for colloidal quantum dot lasers. *NPG Asia Mater.* **2019**, *11*, 41.
- (6) Ithurria, S.; Tessier, M. D.; Mahler, B.; Lobo, R. P. S. M.; Dubertret, B.; Efros, A. L. Colloidal Nanoplatelets with Two-Dimensional Electronic Structure. *Nat. Mater.* **2011**, *10*, 936.
- (7) Pelton, M. Carrier Dynamics, Optical Gain, and Lasing with Colloidal Quantum Wells. *J. Phys. Chem. C* **2018**, *122*, 10659–10674.
- (8) Wang, G.; Chernikov, A.; Glazov, M. M.; Heinz, T. F.; Marie, X.; Amand, T.; Urbaszek, B. Colloquium: Excitons in atomically thin transition metal dichalcogenides. *Rev. Mod. Phys.* **2018**, *90*, 21001.
- (9) Naeem, A.; Masia, F.; Christodoulou, S.; Moreels, I.; Borri, P.; Langbein, W. Giant Exciton Oscillator Strength and Radiatively Limited Dephasing in Two-Dimensional Platelets. *Phys. Rev. B: Condens. Matter Mater. Phys.* **2015**, *91*, 8–12.
- (10) Tomar, R.; Kulkarni, A.; Chen, K.; Singh, S.; Van Thourhout, D.; Hodgkiss, J. M.; Siebbeles, L. D.; Hens, Z.; Geiregat, P. Charge carrier cooling bottleneck opens up nonexcitonic gain mechanisms in colloidal CdSe quantum wells. *J. Phys. Chem. C* **2019**, *123*, 9640–9650.
- (11) Yang, Z.; Pelton, M.; Fedin, I.; Talapin, D. V.; Waks, E. A Room Temperature Continuous-Wave Nanolaser Using Colloidal Quantum Wells. *Nat. Commun.* **2017**, *8*, 1–8.
- (12) Grim, J. Q.; Christodoulou, S.; Di Stasio, F.; Krahn, R.; Cingolani, R.; Manna, L.; Moreels, I. Continuous-wave Biexciton

- Lasing at Room Temperature Using Solution-Processed Quantum Wells. *Nat. Nanotechnol.* **2014**, *9*, 891–895.
- (13) Liu, A.; Jones, R.; Liao, L.; Samara-Rubio, D.; Rubin, D.; Cohen, O.; Nicolaescu, R.; Panizza, M. A high-speed Silicon Optical Modulator Based on a Metal – Oxide – Semiconductor Capacitor. *Nature* **2004**, *427*, 615–618.
- (14) Sun, Z.; Martinez, A.; Wang, F. Optical Modulators with 2D Layered Materials. *Nat. Photonics* **2016**, *10*, 227–238.
- (15) Bennett, B.R.; Soref, R.A.; Del Alamo, J.A. Carrier-Induced Change in Refractive Index of InP, GaAs, and InGaAsP. *IEEE J. Quantum Electron.* **1990**, *26*, 113–122.
- (16) Wang, Z.; Lin, Q.; Wenger, B.; Christoforo, M. G.; Lin, Y.-h.; Klug, M. T.; Johnston, M. B.; Herz, L. M.; Snaith, H. J. High Irradiance Performance of Metal Halide Perovskites for Concentrator Photovoltaics. *Nat. Energy* **2018**, *3*, 855–861.
- (17) Rhodes, W. T.; Adibi, A.; Hänsch, T. W.; Krausz, F.; Monemar, B. A. J.; Venghaus, H.; Weber, H. In *VCSEL: Fundamentals, Technology and Applications of Vertical Cavity Surface-Emitting Lasers*; Michalzik, R., Ed.; Springer: Heidelberg, 2013; Vol. 166, pp 560–561.
- (18) Tamming, R. R.; Butkus, J.; Price, M. B.; Vashishta, P.; Prasad, S. K. K.; Halpert, J. E.; Chen, K.; Hodgkiss, J. M. Ultrafast Spectrally Resolved Photoinduced Complex Refractive Index Changes in CsPbBr₃ Perovskites. *ACS Photonics* **2019**, *6*, 345–350.
- (19) Price, M.; Butkus, J.; Jellicoe, T.; Sadhanala, A.; Briane, A.; Halpert, J.; Broch, K.; Hodgkiss, J.; Friend, R.; Deschler, F. Hot Carrier Cooling and Photo-induced Refractive Index Changes in Organic-Inorganic Lead Halide Perovskites. *Nat. Commun.* **2015**, *6*, 1–8.
- (20) Ghosh, T.; Aharon, S.; Shpatz, A.; Etgar, L.; Ruhman, S. Reflectivity Effects on Pump-Probe Spectra of Lead Halide Perovskites: Comparing Thin Films vs Nanocrystals Reflectivity Effects on Pump-Probe Spectra of Lead Halide Perovskites: Comparing Thin Films vs Nanocrystals. *ACS Nano* **2018**, *12*, 5719–5725.
- (21) Bohn, B. J.; Tong, Y.; Gramlich, M.; Lai, M. L.; Döblinger, M.; Wang, K.; Hoyer, R. L. Z.; Müller-Buschbaum, P.; Stranks, S. D.; Urban, A. S.; Polavarapu, L.; Feldmann, J. Boosting Tunable Blue Luminescence of Halide Perovskite Nanoplatelets Through Post-Synthetic Surface Trap Repair. *Nano Lett.* **2018**, *18*, 5231–5238.
- (22) Weidman, M. C.; Seitz, M.; Stranks, S. D.; Tisdale, W. A. Highly Tunable Colloidal Perovskite Nanoplatelets through Variable Cation, Metal, and Halide Composition. *ACS Nano* **2016**, *10*, 7830–7839.
- (23) Schiettecatte, P.; Geiregat, P.; Hens, Z. Ultrafast Carrier Dynamics in Few-Layer Colloidal Molybdenum Disulfide Probed by Broadband Transient Absorption Spectroscopy. *J. Phys. Chem. C* **2019**, *123*, 10571–10577.
- (24) Zhou, P.; Tanghe, I.; Schiettecatte, P.; Van Thourhout, D.; Hens, Z.; Geiregat, P. Ultrafast carrier dynamics in colloidal WS₂ nanosheets obtained through a hot injection synthesis. *J. Chem. Phys.* **2019**, *151*, 164701.
- (25) Singh, S.; Tomar, R.; ten Brinck, S.; De Roo, J.; Geiregat, P.; Martins, J. C.; Infante, I.; Hens, Z. Colloidal CdSe Nanoplatelets, a Model for Surface Chemistry/Opto-Electronic Property Relations in Semiconductor Nanocrystals. *J. Am. Chem. Soc.* **2018**, *140*, 13292–13300.
- (26) Leemans, J.; Singh, S.; Li, C.; Ten Brinck, S.; Bals, S.; Infante, I.; Moreels, I.; Hens, Z. Near-Edge Ligand Stripping and Robust Radiative Exciton Recombination in CdSe/CdS Core/Crown Nanoplatelets. *J. Phys. Chem. Lett.* **2020**, *11*, 3339–3344.
- (27) Pelant, I.; Valenta, J. In *Luminescence Spectroscopy of Semiconductors*; Oxford University Press, 2012.
- (28) Geiregat, P.; Tomar, R.; Chen, K.; Singh, S.; Hodgkiss, J. M.; Hens, Z. Thermodynamic Equilibrium between Excitons and Excitonic Molecules Dictates Optical Gain in Colloidal CdSe Quantum Wells. *J. Phys. Chem. Lett.* **2019**, *10*, 3637–3644.
- (29) Tokunaga, E.; Terasaki, a.; Kobayashi, T. Frequency-domain Interferometer for Femtosecond Time-resolved Phase Spectroscopy. *Opt. Lett.* **1992**, *17*, 1131–1133.
- (30) Hens, Z.; Moreels, I. Light Absorption by Colloidal Semiconductor Quantum Dots. *J. Mater. Chem.* **2012**, *22*, 10406–10415.
- (31) Alves-Santos, M.; Felice, R. D.; Goldoni, G. Dielectric Functions of Semiconductor Nanoparticles from the Optical Absorption Spectrum: The Case of CdSe and CdS. *J. Phys. Chem. C* **2010**, *114*, 3776–3780.
- (32) Moreels, I.; Allan, G.; De Geyter, B.; Wirtz, L.; Delerue, C.; Hens, Z. Dielectric Function of Colloidal Lead Chalcogenide Quantum Dots Obtained by a Kramers-Krönig Analysis of the Absorbance Spectrum. *Phys. Rev. B: Condens. Matter Mater. Phys.* **2010**, *81*, 1–7.
- (33) Maes, J.; Balcaen, L.; Drijvers, E.; Zhao, Q.; De Roo, J.; Vantomme, A.; Vanhaecke, F.; Geiregat, P.; Hens, Z. Light Absorption Coefficient of CsPbBr₃ Perovskite Nanocrystals. *J. Phys. Chem. Lett.* **2018**, *9*, 3093–3097.
- (34) Achtstein, A. W.; Antanovich, A.; Prudnikau, A.; Scott, R.; Woggon, U.; Artemyev, M. Linear Absorption in CdSe Nanoplates: Thickness and Lateral Size Dependency of the Intrinsic Absorption. *J. Phys. Chem. C* **2015**, *119*, 20156–20161.
- (35) Zhang, Z.; Thung, Y. T.; Chen, X.; Wang, L.; Fan, W.; Ding, L.; Sun, H. Study of Complex Optical Constants of Neat Cadmium Selenide Nanoplatelets Thin Films by Spectroscopic Ellipsometry. *J. Phys. Chem. Lett.* **2021**, *12*, 191–198.
- (36) Bisschop, S.; Geiregat, P.; Aubert, T.; Hens, Z. The Impact of Core/Shell Sizes on the Optical Gain Characteristics of CdSe/CdS Quantum Dots. *ACS Nano* **2018**, *12*, 9011–9021.
- (37) Geiregat, P.; Maes, J.; Chen, K.; Drijvers, E.; De Roo, J.; Hodgkiss, J. M.; Hens, Z. Using Bulk-like Nanocrystals To Probe Intrinsic Optical Gain Characteristics of Inorganic Lead Halide Perovskites. *ACS Nano* **2018**, *12*, 10178–10188.
- (38) Diroll, B. T.; Chen, M.; Coropceanu, I.; Williams, K. R.; Talapin, D. V.; Guyot-Sionnest, P.; Schaller, R. D. Polarized Near-infrared Intersubband Absorptions in CdSe Colloidal Quantum Wells. *Nat. Commun.* **2019**, *10*, 1–9.
- (39) Park, S. H.; Morhange, J. F.; Jeffery, A. D.; Morgan, R. A.; Chavez-Pirson, A.; Gibbs, H. M.; Koch, S. W.; Peyghambarian, N.; Derstine, M.; Gossard, A. C.; English, J. H.; Weigmann, W. Measurements of Room-Temperature Band-Gap-Resonant Optical Nonlinearities of GaAs/AlGaAs Multiple Quantum Wells and Bulk GaAs. *Appl. Phys. Lett.* **1988**, *52*, 1201–1203.
- (40) Garmire, E. Resonant Optical Nonlinearities in Semiconductors. *IEEE J. Sel. Top. Quantum Electron.* **2000**, *6*, 1094–1110.
- (41) Yu, Y.; Yu, Y.; Huang, L.; Peng, H.; Xiong, L.; Cao, L. Giant Gating Tunability of Optical Refractive Index in Transition Metal Dichalcogenide Monolayers. *Nano Lett.* **2017**, *17*, 3613–3618.
- (42) Li, Q.; Lian, T. Area- and Thickness-Dependent Biexciton Auger Recombination in Colloidal CdSe Nanoplatelets: Breaking the “Universal Volume Scaling Law. *Nano Lett.* **2017**, *17*, 3152–3158.
- (43) Kunneman, L. T.; Schins, J. M.; Pedetti, S.; Heuclin, H.; Grozema, F. C.; Houtepen, A. J.; Dubertret, B.; Siebbeles, L. D. A. Nature and Decay Pathways of Photoexcited States in CdSe and CdSe/CdS Nanoplatelets. *Nano Lett.* **2014**, *14*, 7039–7045.
- (44) Pelton, M. Carrier Dynamics, Optical Gain, and Lasing with Colloidal Quantum Wells. *J. Phys. Chem. C* **2018**, *122*, 10659–10674.